

**Radiative power loss calculations for krypton
and argon in intermediate-to-high density
plasmas**

Kevin B. Fournier, Hyun-Kyung Chung and Richard W. Lee

1 December 2001

U. S. Department of Energy

Lawrence
Livermore
National
Laboratory

DISCLAIMER

This document was prepared as an account of work sponsored by an agency of the United States Government. Neither the United States Government nor the University of California nor any of their employees, makes any warranty, express or implied, or assumes any legal liability or responsibility for the accuracy, completeness, or usefulness of any information, apparatus, product, or process disclosed, or represents that its use would not infringe privately owned rights. Reference herein to any specific commercial product, process, or service by trade name, trademark, manufacturer, or otherwise, does not necessarily constitute or imply its endorsement, recommendation, or favoring by the United States Government or the University of California. The views and opinions of authors expressed herein do not necessarily state or reflect those of the United States Government or the University of California, and shall not be used for advertising or product endorsement purposes.

This work was performed under the auspices of the U. S. Department of Energy by the University of California, Lawrence Livermore National Laboratory under Contract No. W-7405-Eng-48.

This report has been reproduced directly from the best available copy.

Available electronically at <http://www.doc.gov/bridge>

Available for a processing fee to U.S. Department of Energy
And its contractors in paper from
U.S. Department of Energy
Office of Scientific and Technical Information
P.O. Box 62
Oak Ridge, TN 37831-0062
Telephone: (865) 576-8401
Facsimile: (865) 576-5728
E-mail: reports@adonis.osti.gov

Available for the sale to the public from
U.S. Department of Commerce
National Technical Information Service
5285 Port Royal Road
Springfield, VA 22161
Telephone: (800) 553-6847
Facsimile: (703) 605-6900
E-mail: orders@ntis.fedworld.gov
Online ordering: <http://www.ntis.gov/ordering.htm>

OR

Lawrence Livermore National Laboratory
Technical Information Department's Digital Library
<http://www.llnl.gov/tid/Library.html>

IACRO number 01-4064
Final report for the period 1 December 2000 to 1 December 2001

Radiative power loss calculations for krypton and argon in intermediate-to-high density plasmas

1 December 2001

Kevin B. Fournier¹, Hyun-Kyung Chung and Richard W. Lee

Lawrence Livermore National Laboratory
P.O. Box 808, L-41
Livermore, CA 94550

This work was performed under the auspices of the U.S. Department of Energy by University of California Lawrence Livermore National Laboratory under contract No. W-7405-Eng-48 and sponsored by the Defense Threat Reduction Agency under DTRA IACRO #01-4064 and Work Unit(s) 01381.

¹ E-mail: fournier2@llnl.gov, phone (925) 423-6129, fax (925) 423-2260

IACRO number 01-4064
Final report for the period 1 December 2000 to 1 December 2001

The scope of work for this subcontract requires that state-of-the-art, detailed atomic kinetics calculations be applied to compute the total radiative cooling rates for Ar and Kr in high density plasmas. This is in support of the Defense Threat Reduction Agency's program of development of simulators with high-fluence radiation and spectral fidelity. Using collisional-radiative modeling codes and unique expertise at Lawrence Livermore National Laboratory (LLNL), the total radiative yields from Ar and Kr, integrated over all photon energies, have been computed. Spectrally resolved yields from K-shell Ar and K- and L-shell Kr have also been tabulated. The present calculations show that high electron density in the plasma sources is essential to maximize the fraction of power output in various x-ray bands.

I. Source Development

The conversion of laser light to multi-kilovolt x-rays is an area of much ongoing research; argon [1] and krypton [2] are used in studies of laser conversion efficiency in under-dense plasmas. Pulsed-power facilities, such as Z-pinches, are the brightest source of multi-kilovolt x-rays currently available; K-shell argon is one of the most important working media in these devices [3,4]. Previous work at LLNL has computed the total radiative yield for Ar [5] and Kr [6] in low-density, magnetically-confined fusion plasmas. These calculations applied detailed, relativistic fine-structure models to the computation of emission from each Ar or Kr ion, as well as state-of-the-art ground configuration ionization and recombination rate data to the calculation of the ionic charge state distribution. Extending these calculation to the regimes of operation of the sources described in Refs. [1-4] requires still larger atomic models accounting for the density-driven satellite transitions, higher- n (Rydberg) configurations and a detailed treatment of ionization and recombination between excited levels.

II. Methods of calculations

The radiative yields for argon and krypton have been computed by calculating the emissivity for all transitions in a detailed model for each charge state, and then summing over the distribution of charge states in equilibrium for some condition. We have computed the collisional-radiative (CR) emission from each argon (Ar^{3+} to Ar^{17+}) and krypton (Kr^{18+} to Kr^{35+}) ion on a grid of six electron densities (1×10^{17} , 1×10^{18} , 1×10^{19} , 1×10^{20} , 1×10^{20} and 1×10^{22} cm^{-3}) for several electron temperatures. All ions with fractional abundance greater than 0.01 % in steady-state equilibrium have been considered for each temperature. The CR emissivity for some transition from level i to level j in each ion is given by

$$I_{i,j}(N_e, T_e, \nu) = h\nu n_i N_e A_{i,j} \quad (1)$$

where $h\nu$ is the transition energy in eV, N_e is the electron density, A_{ij} is the transition rate in s^{-1} for some multipole (E1, E2, M1 or M2) and n_i is the upper level population in relative units of ion density. The steady state upper level population is found by solving the coupled set of rate equations

$$dn_j/dt = 0 = \sum_{i \neq j}^M n_i R_{i,j} - n_j \sum_{i \neq j}^M R_{j,i} \quad (2)$$

where R_{ij} is the rate at which population leaves level i and goes to level j , possibly belonging to a neighboring ion. The sums in equation 2 extend of all M levels considered for all ions at some temperature and density. The atomic data used in equations 1 and 2 are generated with the HULLAC (Hebrew University Lawrence Livermore Atomic Code) suite of codes. HULLAC is built around the fully relativistic atomic structure package RELAC [7,8], and the CROSS [9] suite of codes that computes distorted wave approximation electron impact excitation cross sections. All transitions between bound levels in each argon or krypton ion have been considered for levels with principal quantum numbers $n \leq 6$. As many singly and doubly excited states as possible have been included, this means up to 1700 energy levels for ions in the middle of the L -shell such as the O- and N-like charge states. The HULLAC atomic physics package has recently been modified and extended to produce collisional and photo-ionization cross section in a self-consistent manner with the rest of the atomic data [10]. The HULLAC model can now compute all ionization and recombination rates between all ground and excited levels of an ion and the adjacent ions.

Autoionization rates from highly-excited levels with inner-shell vacancies to all energetically possible levels in the next ion are computed with RELAC [11]. Inner-shell K -shell transitions that are fed by dielectronic recombination (satellites to electron-impact excited resonance lines in He- and H-like ions) have been included in the He- to Ne-like models for both elements. Analogous L -shell transitions that are fed by dielectronic recombination (satellites to resonance transitions in Ne- and F-like ions) have been included in the models for Na- to Ar-like ions. Due to limits on computing resources, the maximum principal quantum number considered for these inner-shell processes has been limited to $n = 4$ or 5. The coupling of adjacent ions as represented by equation 2, and the accounting of inner-shell excited K - and L -shell transitions in the total radiative yield for Ar and Kr are significant extensions of our previous work (i.e. Refs. 5 and 6).

The CR level populations for each Ar and Kr ion have been computed in steady-state according to equation 2 using the atomic kinetics solver CRETIN [12], with accounting for collisional excitation and de-excitation, radiative decays, collisional ionization and autoionization, three-body, dielectronic and radiative recombination. Between 8 and 12 charge states are taken together in the model for a single temperature, and equation 2 is solved for six densities. The charge states chosen for each temperature are selected so that all ions with fractional abundance greater than 0.01 % are included. Detailed, fine-structure atomic data is included for each ion for all levels with principal quantum number $\leq n_{max} = 6$. Rydberg levels up to $n = 10$ are included by averaging over all l -orbital values for each $n_{max} < n \leq 10$. Details about the convergence of our models with principal quantum number, the affect of averaging levels, and the affects of complete coupling of all levels through ionization are being prepared for publication elsewhere [13]. The results presented below are fully converged calculations that are at the limit of what present computation resources can accommodate. Checking indicates that for selected isosequences, our expanded models yield a 30 % enhancement in the total radiative yield above a straight extrapolation of the low density models in Refs. 5 and 6. The details of the calculation for each considered argon and krypton ion are summarized in the Tables I and II.

The power loss coefficient (in eV s⁻¹) for each argon or krypton ion is given by the sum over all transitions

$$L_q^{CR}(N_e, T_e) = \sum_{i,f} I_{i,f} \quad (3)$$

where the subscript q indicates the argon or krypton ion Ar^{q+} or Kr^{q+} . The total volumetric power emitted from, for example, all argon ions in a plasma is given by

$$\begin{aligned} P_{Ar}^{CR}(N_e, T_e) &= \sum_q n_q L_q^{CR}(N_e, T_e) \\ &= N_{Ar} \sum_q f_q(N_e, T_e) L_q^{CR}(N_e, T_e) \end{aligned} \quad (4)$$

where n_q is the density of a particular argon ion, N_{Ar} is the total argon density in the source and f_q is the fractional abundance of argon ion Ar^{q+} , defined by

$$f_q = n_q / N_{Ar} = \sum_j n_j^q / N_{Ar} \quad (5)$$

where the sum over j is over all levels in ion Ar^{q+} . The same formalism applies to our treatment of krypton radiative emission. Details on a pair-wise method of computation of the distribution of charge states that allows for maximum level of detail in the atomic models, and maximum speed will be presented elsewhere [13].

The distribution of argon ion charge states for particular temperature and density conditions has been compared to results from the FLY code [14]. FLY uses detailed models for H- to Li-like ions, and less detailed models for all other iso-electronic sequences, to compute the steady state ion populations of low and mid-Z ($2 \leq Z \leq 26$) elements. This emphasis on accuracy for K -shell models is useful for our validating our argon results. FLY computes the ion populations according to

$$dn_i/dt = \sum_{j=1}^{j=i-1} n_j R_{ji} - n_i R_i + \sum_{j=i+1}^m n_j R_{ji} \quad (6)$$

where m is the total number of levels considered for all iso-electronic sequences, R_{ji} are the rates at which population goes from level j to level i , possibly in a different ion, and R_i are the diagonal elements of the rate matrix that represent the rate at which population leaves level i and goes to all other levels j . Given the resulting distribution of charge states, we compute the average charge on all argon ions for a given temperature and density

$$\langle Z(N_e, T_e) \rangle = \sum_q q f_q(N_e, T_e) \quad (7)$$

We find very close agreement between the $\langle Z \rangle$ our HULLAC data-based models give and the $\langle Z \rangle$ for the same densities and temperatures from FLY. In general, the agreement is much better than 1% for all temperatures above 1000 eV, a range in which K -shell emission is a significant fraction of the total power budget, between 1 – 2 % between 100 and 1000 eV, and better than 5 % at lower temperatures.

We report the last sum in equation 4 as the power loss coefficient and the $\langle Z \rangle$ from equation 7 as results for both Ar and Kr in Tables below. The argon ion density for some given electron density, which is the other term in the last product in equation 4, can be found by dividing the electron density by $\langle Z \rangle$. The power emitted by argon and krypton is also tracked spectrally; we report the K - and L -shell x-ray yields for both elements in the results below.

III. Argon results

Figure 1 shows the calculated radiative yield for line emission from Ar for the range of temperatures from 0.01 to 5.0 keV, and densities from $1.0 \times 10^{17} \text{ cm}^{-3}$ to $1.0 \times 10^{22} \text{ cm}^{-3}$. Clearly defined peaks around 150 eV and 1800 eV, representing yield from *L*- and *K*-shell ions [5], respectively, can be seen in the figure. The units for the ordinate in the figure are $\text{keV s}^{-1} \text{ atom}^{-1}$, one need only multiply by the argon atom density to get the volumetric power ($\text{keV s}^{-1} \text{ cm}^{-3}$), and then by emitting volume to get the total power from the argon plasma. The ion density for a pure argon plasma can be found from the electron density by dividing the electron density by the average ion charge. The average charge from our Ar models is plotted in Fig. 2. The data from Figs. 1 and 2 are listed in Tables III and IV.

For the multi-kilovolt source development work mentioned in Refs. 1 – 4, the *K*-shell yield from Ar is most interesting. Figure 3 shows the spectra for all argon ions predicted by our CR models (equation 2) for several temperatures at $N_e = 1.0 \times 10^{20} \text{ cm}^{-3}$. Clearly, the *K*-shell emission, which is what provides multi-kilovolt yield, is only abundant from plasmas with electron temperatures above 400 eV. Table V lists the *K*-shell yield rate from our argon models, found by summing in equation 3 only over transitions with energies greater than 3 keV. From the data in Fig. 2, *L*-shell ions that have *K*-shell inner-shell transitions are abundant down to temperatures of 100 eV, the *K*-shell output, however, has a strong temperature dependence and is only significant from plasmas with electron temperatures above 400 – 800 eV, depending on the density. The *K*-shell radiative yield rate is shown in Fig. 4. The *K*-shell radiative yield is $\approx 42\%$ of the total output for our lowest density ($1 \times 10^{17} \text{ cm}^{-3}$) run at 1.0 keV, and more than 90 % of the total output for the highest density run ($1 \times 10^{22} \text{ cm}^{-3}$) at 1.0 keV. In like manner, for any given temperature, the x-ray yield is enhanced as a fraction of the total output as the density increases. The fraction of the total output that the x-ray yield represents rises rapidly with increasing temperature, as can be seen in the spectral traces in Fig. 3.

IV. Krypton results

Figure 5 shows the calculated radiative yield for line emission from Kr between 200 eV and 20.0 keV, for densities $1.0 \times 10^{17} \text{ cm}^{-3}$ to $1.0 \times 10^{22} \text{ cm}^{-3}$. The units in the figure are $\text{keV s}^{-1} \text{ atom}^{-1}$, the line emission in equation 3 has been summed over all transition energies. There is less discernable structure in the curves than is the case for argon. The *M*-shell Kr emission occurs for temperatures below 200 eV, and hence, is out of the figure. The *L*- and *K*-shell emission bands from krypton form smooth traces that peak above 600 eV, with the peak moving to higher temperatures at lower densities. The average charge state for the distribution of Kr ions at some temperature (equation 7) is shown for six densities in Fig. 6. From this figure, we can see that the *L*-shell ions (say $\langle Z \rangle \geq 26$) are abundant for temperatures between 600 and 3500 eV. The data shown in Figs. 5 and 6 are listed in Tables VI and VII, respectively.

Spectrally resolved yield calculations are found by limiting the sum in equation 3. Inner-shell *L*- and *K*-shell satellites have been included in all *M*- and *L*-shell ion models, respectively. Hence, there are x-ray contributions to the total power from the *L*- and *K*-shell bands at nearly all temperatures. The calculated *L* + *K*-shell yield for Kr, defined by summing over all transitions with energies greater than or equal to 1.6 keV, is tabulated in Table VIII and shown in Fig. 7. The *K*-shell yield for Kr, defined by

summing over all transitions with energies ≥ 12.0 keV, is tabulated in Table IX and plotted in Fig. 8. Yield from the *K*-shell band is only seen at temperatures near 1500 eV for the highest two densities in our calculations, the inner-shell channel for *K*-shell dielectronic recombination provides this emission. For lower densities, temperatures in excess of 2000 eV are required for *K*-shell yield. The softer yield from the *L*-shell band is seen to be significant for temperatures as low as 600 eV at all densities.

Finally, in Fig. 9, we show the percentage of the total radiative yield that is emitted in the Ar *K*-shell, Kr *L*-shell and Kr *K*-shell bands. For argon, for the highest two densities considered, there is nearly total conversion of the argon output to *K*-shell x-rays; for lower densities, there is less efficient conversion at the same temperatures. For the krypton *L*-shell band (defined as $1.6 \leq E_{\text{photon}} \leq 12.0$ keV), there is greater than 80 % emission for temperatures between 800 and 3500 eV at the two highest densities considered, while the *K*-shell band does not become a significant fraction (≥ 60 %) of the total krypton radiation until the electron temperature is in excess of 10 keV.

V. Summary

We have applied state-of-the-art atomic structure calculations to compute detailed models of radiative emission from argon and krypton. We have solved the steady-state kinetics equations for the level populations in our atomic models for densities ranging from $10^{17} - 10^{22}$ cm⁻³ across a wide range of temperatures. Our models include radiative channels from inner-shell excited *K*- and *L*-shell dielectronic satellite transitions. The effects of high-*n* Rydberg levels have been included in the calculation of the distribution of ion charge states for any given temperature and density. Spectrally resolved tables of ion emission are now available to researchers who are developing multi-kilovolt x-ray sources. The present calculations show that high electron density in the plasma sources is essential to maximize the fraction of power output in various x-ray bands.

The present calculations are only for electron-impact excited line emission and line emission fed by dielectronic recombination. Continuum processes such as Bremsstrahlung and radiative recombination have not been treated. The contributions from these processes can be approximately added to calculations of total yield for some experiment with simple analytical formulae and the tables of $\langle Z \rangle$ that we have computed with our detailed kinetics models. Future work may include improving the calculations for Bremsstrahlung and radiative recombination in a manner that is self-consistent with the rest of this work.

We would further like to apply the present work to on-going DTRA sponsored experiments. We would like to work with developers of hydrodynamics codes such as LASNEX to incorporate our yield calculations in simulations of shots on the OMEGA and HELEN lasers (e.g. work by J. Davis [2] and C. A. Back [1]) to test our models. Tables of emission for individual argon and krypton ions are available [13] (but not listed here) and can be used by researchers simulating non-equilibrium plasmas (such as the work described by Thornhill in Ref. [3]).

Finally, all data in this report are available electronically by request.

References:

- [1] C. A. Back *et al.*, *Bull. Am. Phys. Soc.* **46**, 180-KO2.8 (2001). C. A. Back *et al.*, *X-ray Sources Generated from Gas-filled Laser-Heated Targets* in Atomic Processes in Plasmas: Twelfth Topical Conference, CP547, edited by R. C. Mancini and R. A. Phaneuf. (AIP, Melville, N.Y., 2000).
- [2] J. Davis, *et al.*, *Bull. Am. Phys. Soc.* **46**, 205-KP1.121 (2001).
- [3] H. Sze, *et al.*, *Phys. of Plasmas* **8**, 3135 (2001). J. W. Thornhill, *et al.*, *Phys. of Plasmas* **8**, 3480 (2001).
- [4] H. Sze, *et al.*, *Phys. of Plasmas* **7**, 4223 (2000).
- [5] K. B. Fournier, M. Cohen, M. J. May and W. H. Goldstein, *At. Dat. Nucl. Dat. Tables* **70**, 231 (1998). *Ibid* **74**, 333 (1999).
- [6] K. B. Fournier, M. J. May, D. Pacella, M. Finkenthal, B. C. Gregory and W. H. Goldstein, *Nucl. Fusion* **40**, 847 (2000).
- [7] A. Bar-Shalom and M. Klapisch, *Computer Phys. Commun.* **50**, 375 (1988).
- [8] M. Klapisch, J. L. Schwob, B. S. Fraenkel and J. Oreg, *J. Opt. Soc. Am.* **67**, 148 (1977).
- [9] A. Bar-Shalom, M. Klapisch and J. Oreg, *Phys. Rev. A* **38**, 1773 (1988).
- [10] A. Bar-Shalom, M. Klapisch and J. Oreg, *J. Quant. Spectrosc. Radiat. Transf.* **71**, 169 (2001).
- [11] J. Oreg, W. H. Goldstein and M. Klapisch, *Phys. Rev. A* **44**, 3, 1750 (1991).
- [12] H. A. Scott, *J. Quant. Spectrosc. Radiat. Transf.* **71**, 689 (2001).
- [13] H.-K. Chung, K. B. Fournier and R. W. Lee, *Phys. Rev. E*, in preparation (2002).
- [14] R. W. Lee and J. L. Larsen, *J. Quant. Spectrosc. Radiat. Transf.* **56**, 535 (1996).

Figures:

Figure 1 – Ar radiated power $\text{keV s}^{-1} \text{atom}^{-1}$ for six densities as a function of temperature computed with HULLAC atomic data using CRETIN.

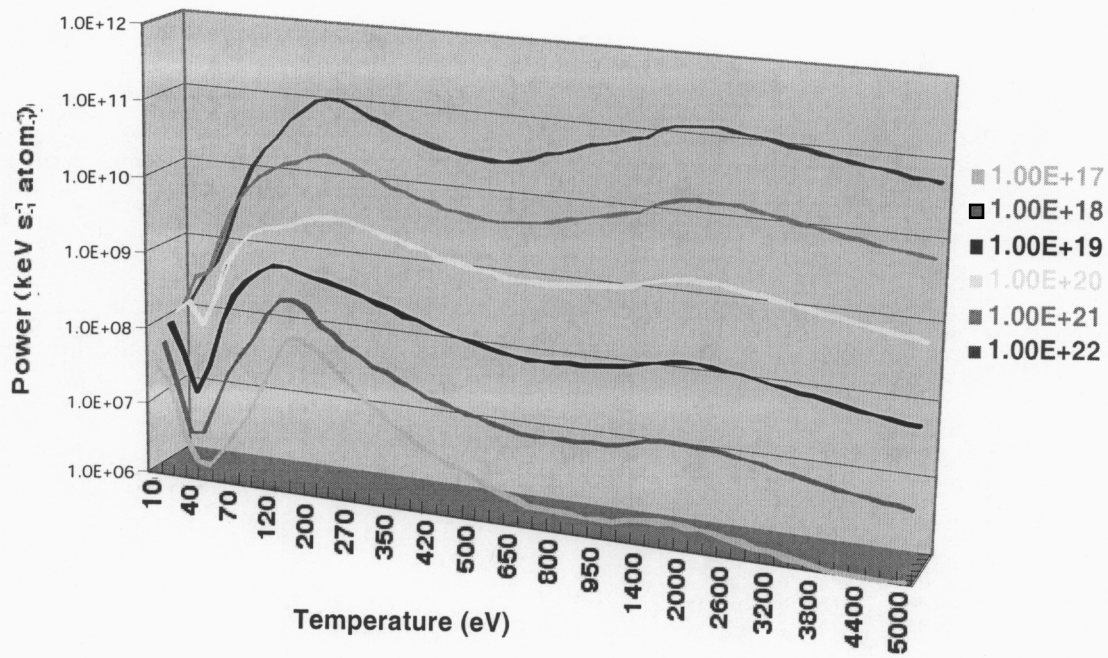


Figure 2 – Average charge on Ar ions as a function of temperature for six densities as computed with our HULLAC-based models using CRETIN.

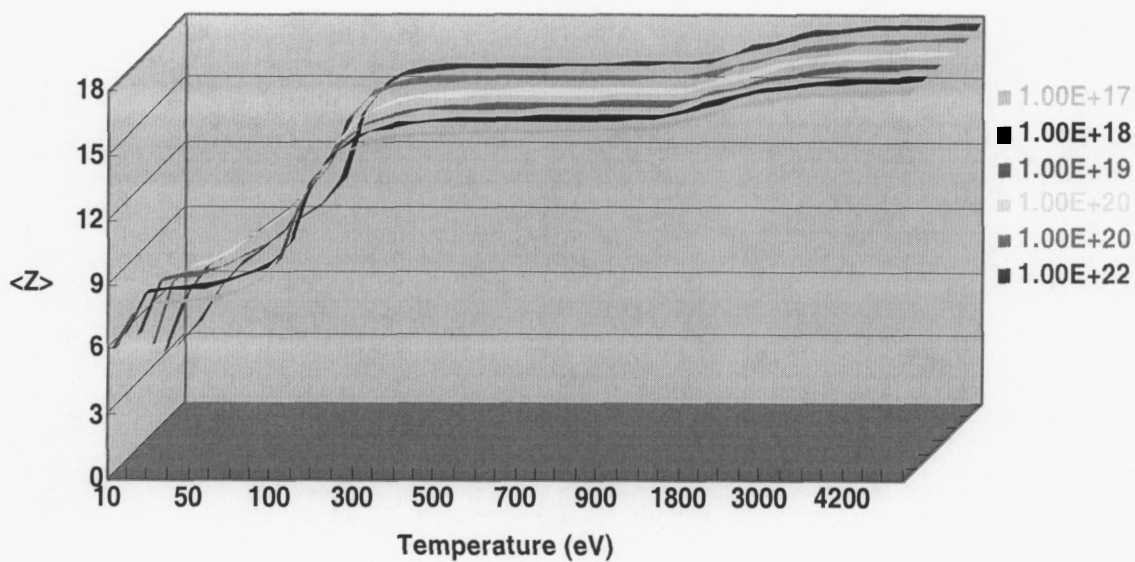


Figure 3 – Ar radiated power $\text{eV s}^{-1} \text{atom}^{-1}$ for $N_e = 1 \times 10^{20} \text{ cm}^{-3}$ at ten electron temperatures computed with HULLAC atomic data using CRETIN.

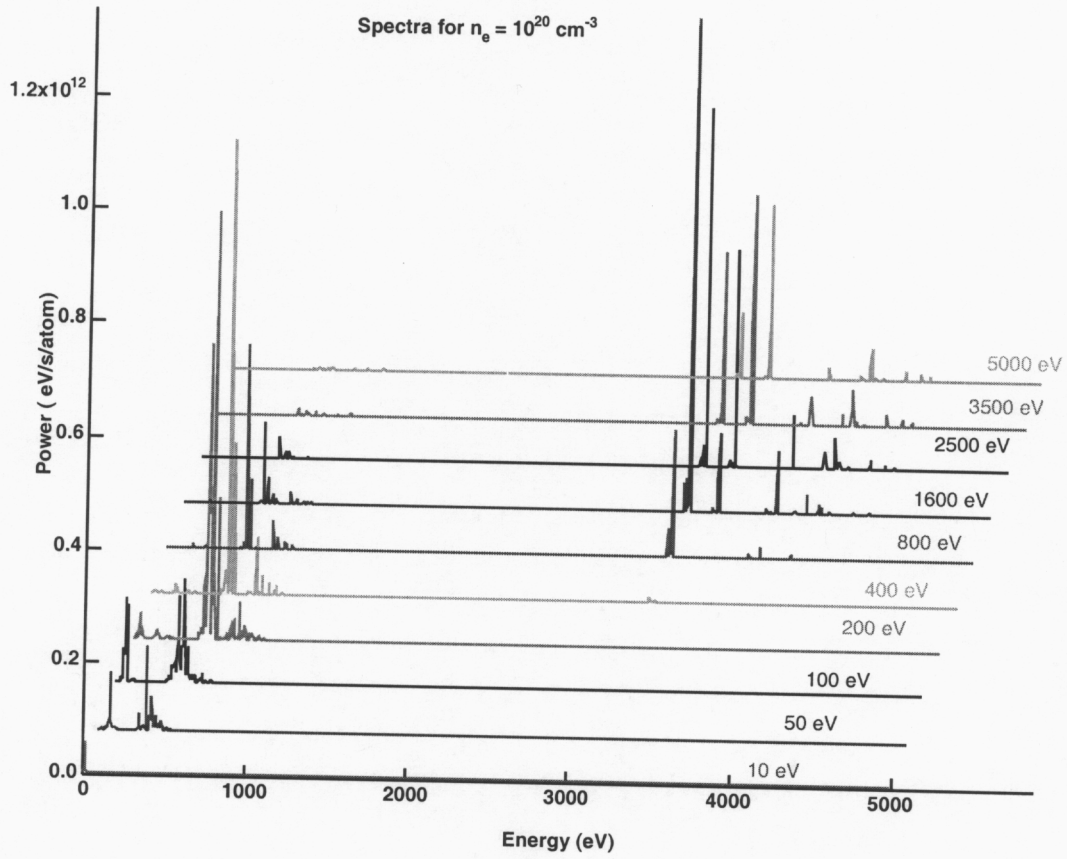


Figure 4 – Ar radiated power $\text{keV s}^{-1} \text{atom}^{-1}$ for six densities as a function of temperature computed with HULLAC atomic data using CRETIN. Only emission from photons with energies $\geq 3.0 \text{ keV}$ is shown.

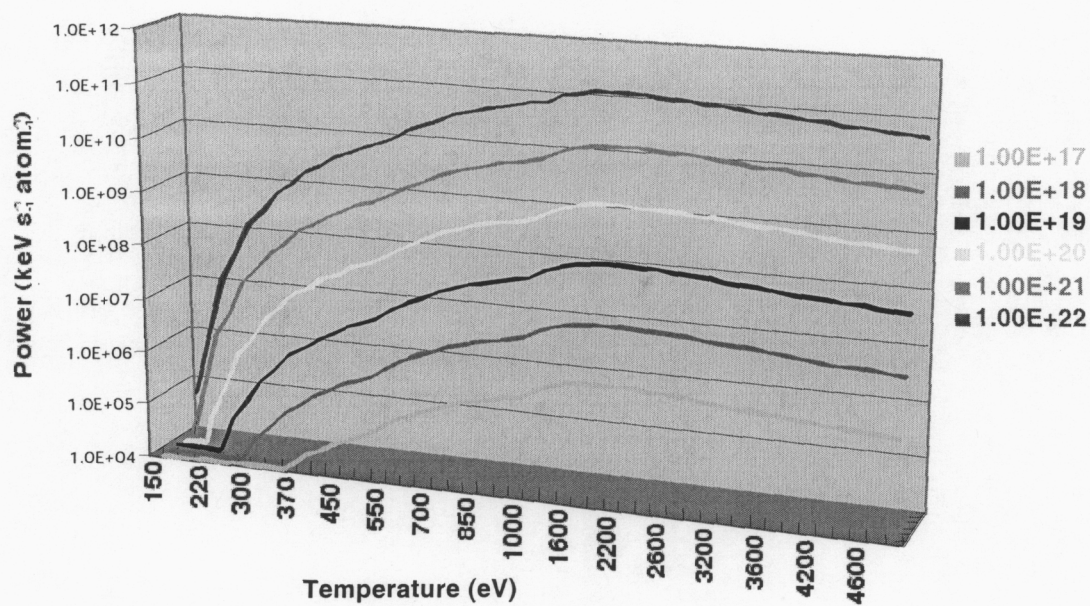


Figure 5 – Kr radiated power $\text{keV s}^{-1} \text{atom}^{-1}$ for six densities as a function of temperature computed with HULLAC atomic data using CRETIN.

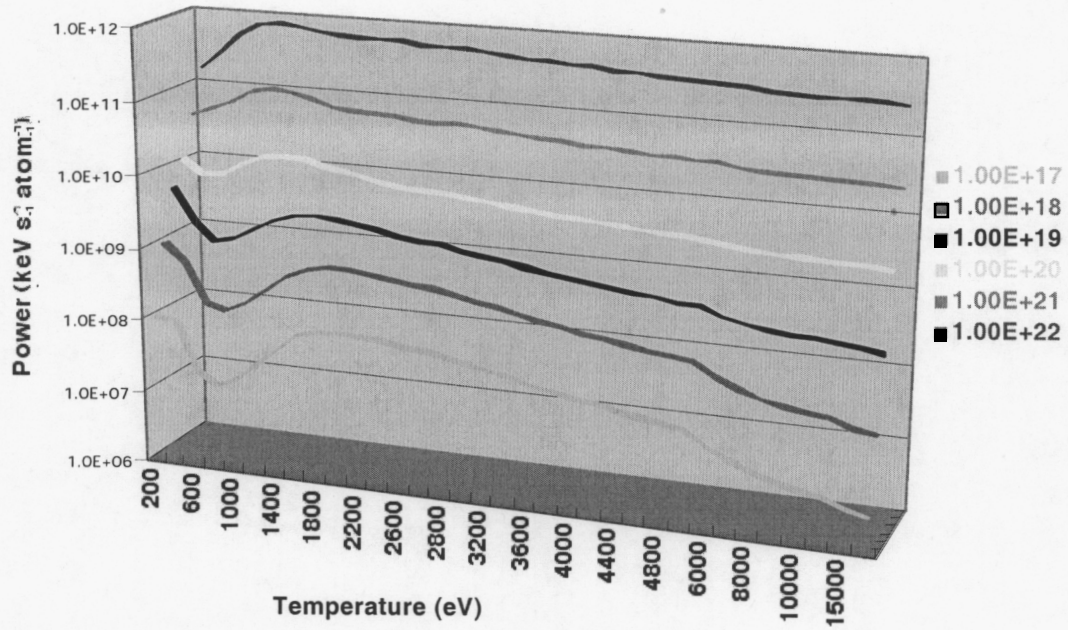


Figure 6 – Average charge on Kr ions as a function of temperature for six densities as computed with our HULLAC-based models using CRETIN.

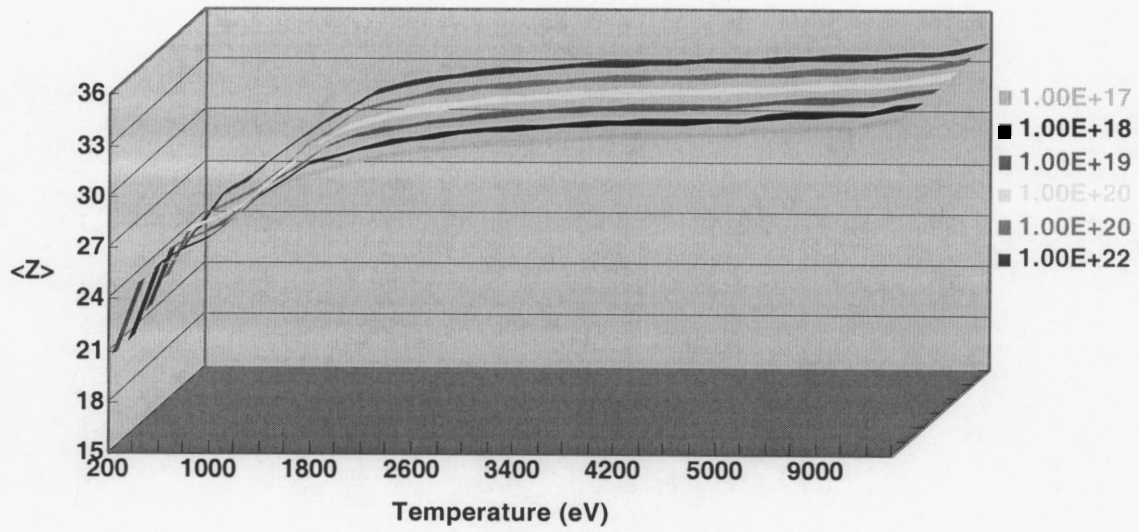


Figure 7 – Kr radiated power $\text{keV s}^{-1} \text{atom}^{-1}$ for six densities as a function of temperature computed with HULLAC atomic data using CRETIN. Only emission from photons with energies $\geq 1.6 \text{ keV}$ is shown.

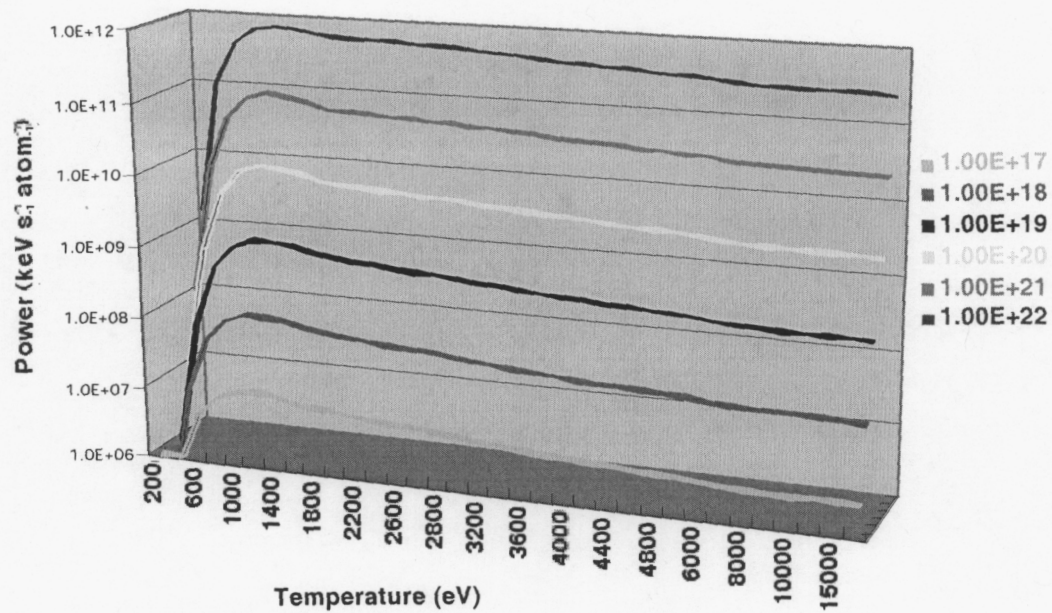
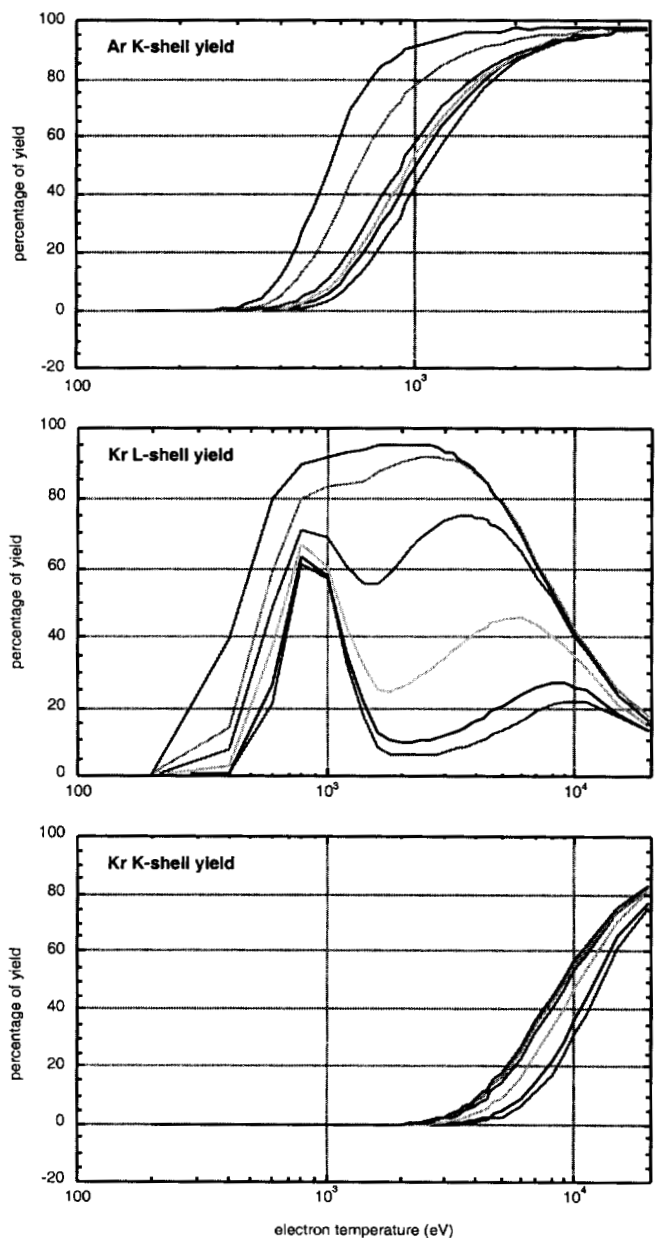


Figure 9 – Percentage of total radiation that comes out in the *K*-shell x-ray band for argon (top), *L*-shell x-ray band (middle) and *K*-shell x-ray band (bottom) for krypton as a function of electron temperature for six densities.



Tables

Table I – HULLAC model details for each argon iso-electronic sequence considered. The second column is the maximum principal quantum number considered for promotion of valence electrons, the third column is the number of configurations considered, the fourth column is the number of detailed levels generated by the considered configurations, the fifth column indicates if inner-shell dielectronic transitions are included, and the maximum principal quantum number considered for capture of the free electron.

<i>Isosequence</i>	n_{max}	<i>No. of configs.</i>	<i>No. of levels</i>	<i>DR channel</i>
H-like	6	20	34	No
He-like	6	47	223	<i>K</i> -shell ($n' < 6$)
Li-like	6	46	333	<i>K</i> -shell ($n' < 6$)
Be-like	6	41	206	<i>K</i> -shell ($n' < 5$)
B-like	6	45	505	<i>K</i> -shell ($n' < 5$)
C-like	6	45	1268	<i>K</i> -shell ($n' < 5$)
N-like	6	45	1737	<i>K</i> -shell ($n' < 5$)
O-like	6	45	1536	<i>K</i> -shell ($n' < 5$)
F-like	5	36	619	<i>K</i> -shell ($n' < 5$)
Ne-like	6	42	231	<i>K</i> -shell ($n' < 5$)
Na-like	6	37	281	<i>L</i> -shell ($n' < 5$)
Mg-like	6	34	197	<i>L</i> -shell ($n' < 4$)
Al-like	6	38	613	<i>L</i> -shell ($n' < 4$)
Si-like	6	38	1475	<i>L</i> -shell ($n' < 4$)
P-like	6	37	1975	<i>L</i> -shell ($n' < 4$)

Table II - HULLAC model details for each krypton iso-electronic sequence considered. The second column is the maximum principal quantum number considered for promotion of valence electrons, the third column is the number of configurations considered, the fourth column is the number of detailed levels generated by the considered configurations, the fifth column indicates if inner-shell dielectronic transitions are included, and the maximum principal quantum number considered for capture of the free electron.

<i>Isosequence</i>	n_{max}	<i>No. of configs.</i>	<i>No. of levels</i>	<i>DR channel</i>
H-like	6	20	34	No
He-like	6	47	223	<i>K-shell</i> ($n' < 6$)
Li-like	6	46	333	<i>K-shell</i> ($n' < 6$)
Be-like	6	41	206	<i>K-shell</i> ($n' < 5$)
B-like	6	45	505	<i>K-shell</i> ($n' < 5$)
C-like	6	45	1268	<i>K-shell</i> ($n' < 5$)
N-like	6	45	1737	<i>K-shell</i> ($n' < 5$)
O-like	6	45	1536	<i>K-shell</i> ($n' < 5$)
F-like	6	44	778	<i>K-shell</i> ($n' < 5$)
Ne-like	6	42	231	<i>K-shell</i> ($n' < 5$)
Na-like	6	37	281	<i>L-shell</i> ($n' < 5$)
Mg-like	6	34	197	<i>L-shell</i> ($n' < 4$)
Al-like	6	38	1012	<i>L-shell</i> ($n' < 4$)
Si-like	6	38	1475	<i>L-shell</i> ($n' < 4$)
P-like	6	37	1975	<i>L-shell</i> ($n' < 4$)
S-like	6	33	1518	<i>L-shell</i> ($n' < 4$)
Cl-like	6	32	752	<i>L-shell</i> ($n' < 4$)
Ar-like	6	29	213	<i>L-shell</i> ($n' < 4$)

Table III – Ar radiated power $\text{keV s}^{-1} \text{atom}^{-1}$ for six densities as a function of temperature computed with HULLAC atomic data using CRETIN.

$N_e \text{ (cm}^{-3}\text{)}$	1.0×10^{17}	1.0×10^{18}	1.0×10^{19}	1.0×10^{20}	1.0×10^{21}	1.0×10^{22}
$T_e \text{ (eV)}$						
10	2.82E+07	5.50E+07	8.93E+07	1.18E+08	1.21E+08	1.18E+08
20	1.71E+07	1.47E+07	3.75E+07	1.68E+08	3.01E+08	2.62E+08
30	3.66E+06	3.53E+06	1.13E+07	8.49E+07	3.90E+08	4.78E+08
40	1.61E+06	3.67E+06	2.80E+07	2.09E+08	1.04E+09	1.08E+09
50	1.59E+06	1.03E+07	1.15E+08	6.23E+08	2.92E+09	4.11E+09
60	2.72E+06	2.73E+07	2.69E+08	1.16E+09	5.48E+09	1.03E+10
70	4.77E+06	5.31E+07	4.38E+08	1.73E+09	8.49E+09	1.77E+10
80	8.32E+06	8.62E+07	6.11E+08	2.09E+09	1.11E+10	2.81E+10
100	2.08E+07	1.92E+08	8.06E+08	2.37E+09	1.39E+10	5.00E+10
120	5.08E+07	3.13E+08	7.99E+08	2.53E+09	1.56E+10	7.01E+10
150	1.11E+08	3.23E+08	6.95E+08	3.05E+09	1.97E+10	9.80E+10
170	1.22E+08	2.69E+08	6.47E+08	3.47E+09	2.06E+10	1.07E+11
200	9.44E+07	1.78E+08	5.73E+08	3.64E+09	1.85E+10	9.77E+10
220	7.33E+07	1.41E+08	5.34E+08	3.55E+09	1.64E+10	8.61E+10
250	4.75E+07	1.01E+08	4.66E+08	3.21E+09	1.35E+10	6.90E+10
270	3.54E+07	8.18E+07	4.19E+08	2.94E+09	1.18E+10	5.95E+10
300	2.31E+07	6.17E+07	3.56E+08	2.54E+09	9.79E+09	4.84E+10
320	1.77E+07	5.21E+07	3.19E+08	2.30E+09	8.74E+09	4.28E+10
350	1.24E+07	4.16E+07	2.73E+08	2.00E+09	7.53E+09	3.65E+10
370	1.00E+07	3.64E+07	2.47E+08	1.83E+09	6.91E+09	3.35E+10
400	7.02E+06	2.89E+07	2.06E+08	1.55E+09	6.07E+09	3.01E+10
420	5.95E+06	2.61E+07	1.90E+08	1.45E+09	5.73E+09	2.86E+10
450	4.79E+06	2.28E+07	1.71E+08	1.32E+09	5.36E+09	2.74E+10
500	3.58E+06	1.91E+07	1.48E+08	1.17E+09	5.05E+09	2.73E+10
550	2.86E+06	1.67E+07	1.34E+08	1.09E+09	5.01E+09	2.90E+10
600	2.42E+06	1.52E+07	1.26E+08	1.04E+09	5.19E+09	3.23E+10
650	2.14E+06	1.43E+07	1.21E+08	1.02E+09	5.52E+09	3.66E+10
700	1.96E+06	1.38E+07	1.19E+08	1.03E+09	5.99E+09	4.19E+10
750	1.85E+06	1.36E+07	1.20E+08	1.05E+09	6.54E+09	4.78E+10
800	1.78E+06	1.37E+07	1.22E+08	1.09E+09	7.17E+09	5.42E+10
850	1.74E+06	1.38E+07	1.25E+08	1.13E+09	7.85E+09	6.09E+10
900	1.73E+06	1.41E+07	1.29E+08	1.19E+09	8.57E+09	6.77E+10
950	1.73E+06	1.45E+07	1.34E+08	1.24E+09	9.31E+09	7.46E+10
1000	1.71E+06	1.47E+07	1.37E+08	1.29E+09	1.00E+10	8.13E+10
1200	1.83E+06	1.66E+07	1.59E+08	1.53E+09	1.29E+10	1.06E+11
1400	1.95E+06	1.83E+07	1.78E+08	1.74E+09	1.52E+10	1.23E+11
1600	2.04E+06	1.95E+07	1.90E+08	1.87E+09	1.67E+10	1.33E+11
1800	2.07E+06	1.99E+07	1.96E+08	1.93E+09	1.75E+10	1.36E+11
2000	2.03E+06	1.97E+07	1.94E+08	1.92E+09	1.75E+10	1.33E+11
2200	1.96E+06	1.91E+07	1.88E+08	1.87E+09	1.71E+10	1.28E+11
2400	1.85E+06	1.81E+07	1.79E+08	1.78E+09	1.63E+10	1.21E+11
2600	1.73E+06	1.70E+07	1.68E+08	1.67E+09	1.53E+10	1.13E+11
3000	1.49E+06	1.47E+07	1.45E+08	1.44E+09	1.33E+10	9.76E+10
3200	1.38E+06	1.36E+07	1.35E+08	1.34E+09	1.24E+10	9.08E+10
3600	1.18E+06	1.17E+07	1.16E+08	1.15E+09	1.07E+10	7.88E+10
4000	1.01E+06	1.00E+07	9.99E+07	9.93E+08	9.29E+09	6.89E+10
4200	9.46E+05	9.38E+06	9.33E+07	9.28E+08	8.70E+09	6.47E+10
4600	8.30E+05	8.24E+06	8.21E+07	8.16E+08	7.68E+09	5.75E+10
5000	7.36E+05	7.32E+06	7.29E+07	7.25E+08	6.84E+09	5.15E+10

Table IV – Average argon ion charge computed from HULLAC-based model using CRETIN.

N_e (cm^{-3})	1.0×10^{17}	1.0×10^{18}	1.0×10^{19}	1.0×10^{20}	1.0×10^{21}	1.0×10^{22}
T_e (eV)						
10	5.78	5.97	5.25	4.18	3.30	3.04
20	7.46	7.83	7.80	7.17	5.81	4.00
30	7.91	7.98	7.98	7.87	7.23	5.70
40	7.97	8.00	8.05	8.08	7.79	6.69
50	8.02	8.08	8.37	8.66	8.45	7.42
60	8.15	8.32	8.89	9.35	9.24	8.19
70	8.44	8.70	9.35	9.97	9.93	8.88
80	8.84	9.10	9.97	10.75	10.69	9.52
100	9.81	10.20	11.42	11.95	12.02	10.73
150	12.44	12.94	13.24	13.58	14.19	13.81
200	14.08	14.24	14.36	14.64	15.23	15.13
250	14.83	14.94	15.02	15.23	15.63	15.60
300	15.27	15.35	15.41	15.54	15.80	15.78
350	15.52	15.58	15.62	15.70	15.87	15.86
400	15.68	15.73	15.75	15.80	15.91	15.90
450	15.77	15.80	15.82	15.85	15.93	15.93
500	15.82	15.84	15.86	15.88	15.95	15.94
550	15.85	15.87	15.88	15.91	15.96	15.96
600	15.88	15.89	15.90	15.92	15.97	15.97
650	15.90	15.91	15.92	15.93	15.97	15.98
700	15.91	15.92	15.93	15.94	15.98	15.99
750	15.93	15.94	15.94	15.95	15.99	16.01
800	15.94	15.95	15.96	15.97	16.00	16.02
850	15.95	15.96	15.97	15.98	16.01	16.04
900	15.97	15.98	15.98	15.99	16.03	16.07
950	15.98	15.99	16.00	16.01	16.04	16.09
1000	16.00	16.01	16.01	16.02	16.06	16.12
1400	16.19	16.21	16.22	16.23	16.28	16.44
1800	16.49	16.51	16.52	16.52	16.59	16.80
2000	16.65	16.67	16.68	16.69	16.75	16.96
2400	16.96	16.97	16.98	16.98	17.04	17.23
2800	17.20	17.21	17.22	17.22	17.27	17.42
3000	17.30	17.31	17.31	17.32	17.35	17.49
3400	17.45	17.46	17.46	17.46	17.49	17.60
3800	17.56	17.57	17.57	17.57	17.59	17.68
4000	17.60	17.61	17.61	17.61	17.63	17.71
4200	17.64	17.64	17.65	17.65	17.66	17.73
4400	17.67	17.67	17.68	17.68	17.69	17.75
4600	17.70	17.70	17.70	17.70	17.72	17.77
5000	17.74	17.75	17.75	17.75	17.76	17.80

Table V – Ar *K*-shell radiated power keV s⁻¹ atom⁻¹ for six densities as a function of temperature computed with HULLAC atomic data. The *K*-shell yield is found by summing over all transitions with energies greater than 3.0 keV.

N_e (cm ⁻³)	1.0×10 ¹⁷	1.0×10 ¹⁸	1.0×10 ¹⁹	1.0×10 ²⁰	1.0×10 ²¹	1.0×10 ²²
T_e (eV)						
150	2.38E-01	2.08E+00	2.23E+01	2.73E+02	7.14E+03	5.93E+04
170	1.54E+00	1.32E+01	1.45E+02	2.17E+03	8.18E+04	7.71E+05
200	1.44E+01	1.63E+02	1.94E+03	3.32E+04	1.05E+06	1.10E+07
220	5.66E+01	6.82E+02	8.05E+03	1.31E+05	3.42E+06	3.68E+07
250	3.15E+02	3.76E+03	4.27E+04	6.18E+05	1.27E+07	1.39E+08
270	7.81E+02	9.07E+03	1.01E+05	1.37E+06	2.49E+07	2.74E+08
300	2.30E+03	2.57E+04	2.78E+05	3.51E+06	5.62E+07	6.18E+08
320	4.09E+03	4.49E+04	4.79E+05	5.83E+06	8.78E+07	9.64E+08
350	8.34E+03	8.95E+04	9.41E+05	1.10E+07	1.55E+08	1.69E+09
370	1.24E+04	1.32E+05	1.37E+06	1.58E+07	2.14E+08	2.33E+09
400	2.09E+04	2.19E+05	2.26E+06	2.53E+07	3.27E+08	3.53E+09
420	2.80E+04	2.91E+05	3.00E+06	3.31E+07	4.19E+08	4.51E+09
450	4.10E+04	4.23E+05	4.34E+06	4.73E+07	5.83E+08	6.23E+09
470	5.14E+04	5.27E+05	5.40E+06	5.85E+07	7.09E+08	7.56E+09
500	6.95E+04	7.10E+05	7.25E+06	7.79E+07	9.26E+08	9.81E+09
550	1.07E+05	1.08E+06	1.10E+07	1.17E+08	1.36E+09	1.42E+10
600	1.52E+05	1.54E+06	1.56E+07	1.65E+08	1.87E+09	1.94E+10
650	2.06E+05	2.08E+06	2.10E+07	2.20E+08	2.46E+09	2.53E+10
700	2.66E+05	2.68E+06	2.71E+07	2.82E+08	3.11E+09	3.16E+10
750	3.33E+05	3.35E+06	3.38E+07	3.50E+08	3.81E+09	3.84E+10
800	4.05E+05	4.07E+06	4.10E+07	4.24E+08	4.56E+09	4.55E+10
850	4.82E+05	4.83E+06	4.87E+07	5.01E+08	5.34E+09	5.28E+10
900	5.61E+05	5.63E+06	5.66E+07	5.81E+08	6.14E+09	6.01E+10
950	6.43E+05	6.44E+06	6.47E+07	6.63E+08	6.96E+09	6.73E+10
1000	7.26E+05	7.26E+06	7.30E+07	7.45E+08	7.77E+09	7.44E+10
1200	1.05E+06	1.05E+07	1.05E+08	1.07E+09	1.09E+10	9.96E+10
1400	1.34E+06	1.33E+07	1.33E+08	1.34E+09	1.34E+10	1.18E+11
1600	1.56E+06	1.54E+07	1.54E+08	1.55E+09	1.52E+10	1.28E+11
1800	1.69E+06	1.67E+07	1.66E+08	1.67E+09	1.61E+10	1.31E+11
2000	1.74E+06	1.71E+07	1.70E+08	1.71E+09	1.64E+10	1.30E+11
2200	1.73E+06	1.70E+07	1.69E+08	1.69E+09	1.61E+10	1.24E+11
2400	1.67E+06	1.65E+07	1.64E+08	1.63E+09	1.55E+10	1.18E+11
2500	1.63E+06	1.61E+07	1.60E+08	1.60E+09	1.51E+10	1.14E+11
2600	1.59E+06	1.57E+07	1.56E+08	1.55E+09	1.46E+10	1.10E+11
2800	1.50E+06	1.47E+07	1.46E+08	1.46E+09	1.37E+10	1.03E+11
3000	1.40E+06	1.38E+07	1.37E+08	1.37E+09	1.28E+10	9.54E+10
3200	1.30E+06	1.28E+07	1.28E+08	1.27E+09	1.20E+10	8.87E+10
3400	1.21E+06	1.19E+07	1.19E+08	1.18E+09	1.11E+10	8.26E+10
3500	1.17E+06	1.15E+07	1.15E+08	1.14E+09	1.07E+10	7.98E+10
3600	1.13E+06	1.11E+07	1.11E+08	1.10E+09	1.04E+10	7.71E+10
3800	1.04E+06	1.03E+07	1.03E+08	1.02E+09	9.64E+09	7.20E+10
4000	9.79E+05	9.69E+06	9.64E+07	9.61E+08	9.05E+09	6.75E+10
4200	9.11E+05	9.02E+06	8.98E+07	8.96E+08	8.45E+09	6.33E+10
4400	8.54E+05	8.47E+06	8.43E+07	8.40E+08	7.93E+09	5.96E+10
4500	8.31E+05	8.24E+06	8.21E+07	8.18E+08	7.72E+09	5.80E+10
4600	8.03E+05	7.96E+06	7.93E+07	7.90E+08	7.47E+09	5.63E+10
4800	7.56E+05	7.50E+06	7.47E+07	7.45E+08	7.05E+09	5.33E+10
5000	7.17E+05	7.11E+06	7.09E+07	7.06E+08	6.68E+09	5.06E+10

Table VI – Kr radiated power keV s⁻¹ atom⁻¹ for six densities as a function of temperature computed with HULLAC atomic data using CRETIN.

N_e (cm ⁻³)	1.0×10 ¹⁷	1.0×10 ¹⁸	1.0×10 ¹⁹	1.0×10 ²⁰	1.0×10 ²¹	1.0×10 ²²
T_e (eV)						
200	1.11E+08	1.04E+09	5.29E+09	1.11E+10	4.14E+10	1.71E+11
400	1.06E+08	5.92E+08	1.88E+09	7.71E+09	5.35E+10	2.72E+11
600	2.17E+07	1.64E+08	1.06E+09	8.02E+09	6.94E+10	5.10E+11
800	1.47E+07	1.39E+08	1.27E+09	1.16E+10	1.02E+11	7.44E+11
1000	1.96E+07	1.92E+08	1.80E+09	1.52E+10	1.17E+11	7.99E+11
1200	3.44E+07	3.13E+08	2.50E+09	1.64E+10	1.07E+11	7.37E+11
1400	6.02E+07	4.85E+08	3.05E+09	1.55E+10	9.04E+10	6.74E+11
1600	1.02E+08	7.04E+08	3.22E+09	1.27E+10	7.30E+10	6.07E+11
1800	1.19E+08	7.69E+08	3.06E+09	1.14E+10	6.98E+10	6.03E+11
2000	1.24E+08	7.65E+08	2.76E+09	1.03E+10	6.70E+10	5.92E+11
2200	1.19E+08	7.16E+08	2.46E+09	9.37E+09	6.45E+10	5.75E+11
2400	1.09E+08	6.47E+08	2.16E+09	8.57E+09	6.17E+10	5.53E+11
2600	9.74E+07	5.73E+08	1.90E+09	7.87E+09	5.87E+10	5.28E+11
2600	9.74E+07	5.73E+08	1.90E+09	7.87E+09	5.87E+10	5.28E+11
2800	8.55E+07	5.03E+08	1.68E+09	7.26E+09	5.57E+10	5.03E+11
3000	7.45E+07	4.39E+08	1.49E+09	6.72E+09	5.29E+10	4.79E+11
3200	6.48E+07	3.84E+08	1.32E+09	6.26E+09	5.03E+10	4.57E+11
3400	5.63E+07	3.36E+08	1.19E+09	5.86E+09	4.79E+10	4.36E+11
3600	4.86E+07	2.93E+08	1.06E+09	5.48E+09	4.55E+10	4.16E+11
3800	4.26E+07	2.59E+08	9.70E+08	5.18E+09	4.36E+10	4.00E+11
4000	3.74E+07	2.30E+08	8.90E+08	4.92E+09	4.19E+10	3.85E+11
4200	3.31E+07	2.06E+08	8.21E+08	4.70E+09	4.04E+10	3.73E+11
4400	2.94E+07	1.85E+08	7.63E+08	4.50E+09	3.91E+10	3.62E+11
4600	2.63E+07	1.68E+08	7.12E+08	4.33E+09	3.80E+10	3.52E+11
4800	2.33E+07	1.51E+08	6.63E+08	4.15E+09	3.67E+10	3.42E+11
5000	2.11E+07	1.38E+08	6.26E+08	4.03E+09	3.58E+10	3.34E+11
6000	1.36E+07	9.48E+07	4.99E+08	3.57E+09	3.27E+10	3.09E+11
7000	9.71E+06	7.17E+07	4.28E+08	3.32E+09	3.10E+10	2.96E+11
8000	7.33E+06	5.71E+07	3.81E+08	3.14E+09	2.98E+10	2.87E+11
9000	6.02E+06	4.91E+07	3.56E+08	3.06E+09	2.93E+10	2.84E+11
10000	5.17E+06	4.38E+07	3.39E+08	3.00E+09	2.90E+10	2.82E+11
11000	4.60E+06	4.02E+07	3.27E+08	2.97E+09	2.88E+10	2.81E+11
15000	3.45E+06	3.25E+07	2.97E+08	2.85E+09	2.80E+10	2.76E+11
20000	2.93E+06	2.85E+07	2.75E+08	2.69E+09	2.66E+10	2.64E+11

Table VII – Average krypton ion charge computed from HULLAC-based model using CRETIN.

N_e (cm^{-3})	1.0×10^{17}	1.0×10^{18}	1.0×10^{19}	1.0×10^{20}	1.0×10^{21}	1.0×10^{22}
T_e (eV)						
200	20.46	20.61	21.39	22.36	22.99	23.40
400	24.74	24.80	25.00	25.17	25.34	25.63
600	25.80	25.78	25.78	25.83	25.95	26.45
800	26.45	26.45	26.47	26.57	26.77	27.64
1000	27.59	27.60	27.66	27.80	28.01	28.85
1200	28.85	28.87	28.96	29.13	29.33	29.91
1400	29.81	29.84	29.97	30.18	30.38	30.75
1600	30.79	30.85	30.99	31.20	31.36	31.54
1800	31.26	31.33	31.48	31.66	31.81	31.95
2000	31.66	31.73	31.86	32.03	32.15	32.27
2200	31.96	32.03	32.15	32.30	32.41	32.51
2400	32.21	32.28	32.39	32.51	32.61	32.70
2600	32.42	32.48	32.57	32.69	32.77	32.86
2800	32.59	32.64	32.73	32.83	32.91	32.98
3000	32.74	32.78	32.86	32.95	33.02	33.09
3200	32.86	32.90	32.97	33.05	33.11	33.17
3400	32.97	33.00	33.06	33.14	33.19	33.25
3600	33.06	33.09	33.15	33.22	33.26	33.32
3800	33.14	33.16	33.21	33.28	33.32	33.37
4000	33.21	33.23	33.27	33.33	33.37	33.42
4200	33.26	33.28	33.32	33.38	33.42	33.46
4400	33.32	33.33	33.37	33.42	33.46	33.49
4600	33.36	33.38	33.41	33.46	33.49	33.53
4800	33.41	33.42	33.45	33.50	33.53	33.56
5000	33.44	33.45	33.48	33.53	33.55	33.58
6000	33.58	33.59	33.61	33.64	33.67	33.69
7000	33.68	33.69	33.70	33.73	33.75	33.76
8000	33.76	33.77	33.78	33.80	33.82	33.83
9000	33.83	33.83	33.84	33.86	33.87	33.89
10000	33.89	33.89	33.90	33.92	33.93	33.94
15000	34.15	34.16	34.16	34.17	34.18	34.19
20000	34.40	34.40	34.40	34.41	34.41	34.42

Table VIII – Kr $L + K$ -shell radiated power $\text{keV s}^{-1} \text{atom}^{-1}$ for six densities as a function of temperature computed with HULLAC atomic data. The yield for this table is computed by summing over all transitions with energies greater than 1.6 keV.

$N_e \text{ (cm}^{-3}\text{)}$	1.0×10^{17}	1.0×10^{18}	1.0×10^{19}	1.0×10^{20}	1.0×10^{21}	1.0×10^{22}
$T_e \text{ (eV)}$						
200	1.02E+04	1.04E+05	1.12E+06	1.05E+07	1.20E+08	1.51E+09
400	8.66E+05	7.27E+06	5.98E+07	6.05E+08	7.66E+09	1.08E+11
600	4.53E+06	4.37E+07	3.99E+08	3.89E+09	4.12E+10	4.07E+11
800	8.88E+06	8.80E+07	8.46E+08	8.24E+09	8.13E+10	6.64E+11
1000	1.12E+07	1.11E+08	1.09E+09	1.04E+10	9.82E+10	7.34E+11
1200	1.11E+07	1.11E+08	1.07E+09	9.90E+09	8.97E+10	6.86E+11
1400	1.04E+07	1.03E+08	9.79E+08	8.66E+09	7.67E+10	6.33E+11
1600	8.70E+06	8.57E+07	7.98E+08	7.00E+09	6.35E+10	5.77E+11
1800	8.15E+06	8.04E+07	7.51E+08	6.70E+09	6.21E+10	5.76E+11
2000	7.54E+06	7.44E+07	7.03E+08	6.43E+09	6.07E+10	5.66E+11
2200	7.01E+06	6.94E+07	6.62E+08	6.18E+09	5.91E+10	5.51E+11
2400	6.52E+06	6.47E+07	6.23E+08	5.90E+09	5.69E+10	5.30E+11
2600	6.06E+06	6.03E+07	5.86E+08	5.62E+09	5.45E+10	5.07E+11
2600	6.06E+06	6.03E+07	5.86E+08	5.62E+09	5.45E+10	5.07E+11
2800	5.65E+06	5.63E+07	5.51E+08	5.33E+09	5.20E+10	4.83E+11
3000	5.29E+06	5.27E+07	5.19E+08	5.06E+09	4.95E+10	4.61E+11
3200	4.96E+06	4.95E+07	4.90E+08	4.81E+09	4.72E+10	4.39E+11
3400	4.68E+06	4.68E+07	4.64E+08	4.58E+09	4.51E+10	4.20E+11
3600	4.40E+06	4.39E+07	4.38E+08	4.35E+09	4.29E+10	4.00E+11
3800	4.18E+06	4.18E+07	4.18E+08	4.17E+09	4.12E+10	3.85E+11
4000	4.00E+06	4.00E+07	4.00E+08	4.01E+09	3.97E+10	3.72E+11
4200	3.84E+06	3.84E+07	3.85E+08	3.86E+09	3.84E+10	3.60E+11
4400	3.70E+06	3.70E+07	3.72E+08	3.74E+09	3.72E+10	3.49E+11
4600	3.57E+06	3.58E+07	3.60E+08	3.63E+09	3.61E+10	3.40E+11
4800	3.44E+06	3.45E+07	3.47E+08	3.51E+09	3.50E+10	3.31E+11
5000	3.35E+06	3.36E+07	3.39E+08	3.43E+09	3.42E+10	3.24E+11
6000	3.04E+06	3.05E+07	3.08E+08	3.14E+09	3.14E+10	3.00E+11
7000	2.89E+06	2.89E+07	2.93E+08	2.98E+09	3.00E+10	2.89E+11
8000	2.79E+06	2.79E+07	2.82E+08	2.88E+09	2.89E+10	2.81E+11
9000	2.76E+06	2.76E+07	2.79E+08	2.84E+09	2.86E+10	2.78E+11
10000	2.74E+06	2.75E+07	2.77E+08	2.82E+09	2.83E+10	2.77E+11
11000	2.74E+06	2.75E+07	2.77E+08	2.81E+09	2.82E+10	2.77E+11
15000	2.71E+06	2.71E+07	2.73E+08	2.76E+09	2.77E+10	2.74E+11
20000	2.61E+06	2.61E+07	2.62E+08	2.64E+09	2.64E+10	2.62E+11

Table IX – Kr *K*-shell radiated power keV s⁻¹ atom⁻¹ for six densities as a function of temperature computed with HULLAC atomic data. The *K*-shell yield is computed by summing over all transitions with energies greater than 12.0 keV.

N_e (cm ⁻³)	1.0×10 ¹⁷	1.0×10 ¹⁸	1.0×10 ¹⁹	1.0×10 ²⁰	1.0×10 ²¹	1.0×10 ²²
T_e (eV)						
200	1.83E-30	4.39E-29	8.95E-27	1.27E-24	1.37E-22	3.79E-20
400	1.94E-09	1.97E-08	2.54E-07	3.98E-06	8.86E-05	8.17E-03
600	1.44E-03	1.44E-02	1.58E-01	1.99E+00	3.10E+01	1.67E+03
800	1.25E+00	1.26E+01	1.33E+02	1.43E+03	1.68E+04	4.41E+05
1000	6.92E+01	6.89E+02	6.76E+03	6.01E+04	5.67E+05	8.52E+06
1200	7.51E+02	7.27E+03	6.47E+04	4.93E+05	4.21E+06	4.78E+07
1400	3.25E+03	3.01E+04	2.41E+05	1.66E+06	1.38E+07	1.42E+08
1600	9.10E+03	7.81E+04	5.59E+05	3.79E+06	3.30E+07	3.44E+08
1800	1.71E+04	1.42E+05	9.99E+05	7.34E+06	6.84E+07	7.43E+08
2000	2.78E+04	2.27E+05	1.66E+06	1.37E+07	1.35E+08	1.50E+09
2200	4.12E+04	3.41E+05	2.65E+06	2.40E+07	2.45E+08	2.72E+09
2400	5.80E+04	4.93E+05	4.08E+06	3.92E+07	4.07E+08	4.50E+09
2600	7.87E+04	6.88E+05	6.02E+06	6.00E+07	6.25E+08	6.85E+09
2600	7.87E+04	6.88E+05	6.02E+06	6.00E+07	6.25E+08	6.85E+09
2800	1.04E+05	9.30E+05	8.47E+06	8.62E+07	8.98E+08	9.75E+09
3000	1.33E+05	1.22E+06	1.14E+07	1.18E+08	1.22E+09	1.31E+10
3200	1.66E+05	1.55E+06	1.48E+07	1.53E+08	1.59E+09	1.69E+10
3400	2.03E+05	1.92E+06	1.86E+07	1.93E+08	1.99E+09	2.11E+10
3600	2.44E+05	2.33E+06	2.29E+07	2.37E+08	2.44E+09	2.57E+10
3800	2.87E+05	2.77E+06	2.73E+07	2.82E+08	2.90E+09	3.03E+10
4000	3.32E+05	3.22E+06	3.19E+07	3.30E+08	3.38E+09	3.52E+10
4200	3.78E+05	3.69E+06	3.67E+07	3.78E+08	3.87E+09	4.01E+10
4400	4.27E+05	4.18E+06	4.17E+07	4.28E+08	4.37E+09	4.52E+10
4600	4.76E+05	4.67E+06	4.67E+07	4.79E+08	4.88E+09	5.03E+10
4800	5.26E+05	5.19E+06	5.19E+07	5.31E+08	5.40E+09	5.55E+10
5000	5.76E+05	5.69E+06	5.69E+07	5.82E+08	5.91E+09	6.06E+10
6000	8.24E+05	8.18E+06	8.20E+07	8.33E+08	8.41E+09	8.55E+10
7000	1.06E+06	1.05E+07	1.06E+08	1.07E+09	1.07E+10	1.08E+11
8000	1.27E+06	1.27E+07	1.27E+08	1.28E+09	1.28E+10	1.29E+11
9000	1.46E+06	1.45E+07	1.45E+08	1.46E+09	1.46E+10	1.47E+11
10000	1.62E+06	1.61E+07	1.61E+08	1.62E+09	1.61E+10	1.62E+11
11000	1.75E+06	1.75E+07	1.75E+08	1.75E+09	1.75E+10	1.75E+11
15000	2.11E+06	2.11E+07	2.10E+08	2.09E+09	2.08E+10	2.08E+11
20000	2.24E+06	2.24E+07	2.23E+08	2.22E+09	2.20E+10	2.20E+11

DISTRIBUTION LIST:

John Davis, Alme & Associates, Suite 204, 6020 S. Richmond Hwy, Alexandria, VA 22303-2157

Christina Back, PO Box 808, L-021, Lawrence Livermore National Laboratory, Livermore, CA 94550

Larry Suter, PO Box 808, L-031, Lawrence Livermore National Laboratory, Livermore, CA 94550

Michael C. Miller, PO Box 808, L-183, Lawrence Livermore National Laboratory, Livermore, CA
94550

Todd J. Hoover, PO Box 808, L-015, Lawrence Livermore National Laboratory, Livermore, CA 94550